Conductance-Based Phenomenological Nonspiking Model: A Dimensionless and Simple Model That Reliably Predicts the Effects of Conductance Variations on Nonspiking Neuronal Dynamics

Loïs Naudin, Laetitia Raison-Aubry, Laure Buhry

Conductance-based phenomenological non-spiking model: a dimensionless and simple model that reliably predicts the effects of conductance variations on non-spiking neuronal dynamics

Loïs Naudin[1*+], Laetitia Raison-Aubry[1+], and Laure Buhry[1]

[1]Laboratoire Lorrain de Recherche en Informatique et ses Applications, CNRS, Université de Lorraine, Nancy, France

[*]Corresponding author: lois.naudin@gmail.com

[+]These authors contributed equally (joint first author)

October 15, 2023

Abstract

The modeling of single neurons has proven to be an indispensable tool in deciphering the mechanisms underlying neural dynamics and signal processing. In that sense, two types of single-neuron models are extensively used: the conductance-based models (CBMs) and the so-called 'phenomenological' models, which are often opposed in their objectives and their use. Indeed, the first type aims to describe the biophysical properties of the neuron cell membrane that underlie the evolution of its potential, while the second one describes the macroscopic behavior of the neuron without taking into account all its underlying physiological processes. Therefore, CBMs are often used to study 'low-level' functions of neural systems, while phenomenological models are limited to the description of 'high-level' functions. In this paper, we develop a numerical procedure to endow a dimensionless and simple phenomenological non-spiking model with the capability to describe the effect of conductance variations on non-spiking neuronal dynamics with high accuracy. The procedure allows to determine a relationship between the dimensionless parameters of the phenomenological

model and the maximal conductances of CBMs. In this way, the simple model combines the biological plausibility of CBMs with the high computational efficiency of phenomenological models, and thus may serve as a building block for studying both 'high-level' and 'low-level' functions of non-spiking neural networks. We also demonstrate this capability in an abstract neural network inspired by the retina and *C. elegans* networks, two important non-spiking nervous tissues.

Keywords: Simple neuron model; non-spiking neurons; conductance variations; bifurcation; *Caenorhabditis elegans*; retina.

1 Introduction

To better understand how neuronal circuits control behavior and brain functions, neuron modeling is a widely-used tool. Two types of models characterizing the dynamics of single neurons can be used. The first one is the conductance-based model (CBM), which inherits the Hodgkin-Huxley formalism (Hodgkin and Huxley, 1952) and aims to describe the biophysical properties of the neuron cell membrane that underlie the evolution of its potential. In this model, every individual parameter and state variable has an established electrophysiological meaning. Therefore, CBMs are broadly used to understand 'low-level' functions of neural systems (Eliasmith and Trujillo, 2014; O'Leary et al., 2015), such as monitoring the effects of specific conductance variations on neuronal dynamics (Giovannini et al., 2017; Poirazi and Papoutsi, 2020; Naudin et al., 2022c), or modeling gain- or loss-of-function mutations in genes encoding ion channels (Lemaire et al., 2021).

The second type of model is often qualified by the term 'phenomenological', although some authors contradict it (Brette, 2015). This type of model was developed in part to overcome the drawbacks of CBMs, which are twofold: (i) they have a very high computational cost due to their complexity so that only a handful of neurons can be simulated in real time (Izhikevich, 2004), and (ii) the insights obtained from a mathematical analysis are quite limited as these are high-dimensional systems (Ermentrout and Terman, 2010). A phenomenological model therefore aims to be lightweight, simple, and to describe the macroscopic behavior of the neuron without taking into account all its underlying physiological processes. Some classical examples are the FitzHugh–Nagumo model (FitzHugh, 1961), Izhikevich model (Izhikevich, 2003), or many integrate-and-fire models (Latham et al., 2000; Smith et al., 2000; Górski et al., 2021). The counterpart of phenomenological models is that their parameters are dimensionless, thus limited to the study of 'high-level' functions of neural systems.

A simple phenomenological model of non-spiking neurons was recently developed in Naudin et al. (2022b). This type of neuron is found in a wide variety of nervous tissues (Davis and Stretton, 1989b; Goodman et al., 1998; Field and Chichilnisky, 2007), encodes neuronal information in an analog manner through graded responses (Lockery et al., 2009), and plays a crucial role in the functioning of many nervous systems (Roberts and Bush, 1981; Burrows et al., 1988; Laurent and Burrows, 1989; Davis and Stretton, 1989a; Bidaye et al., 2018). Further, three phenotypes of non-spiking neurons can be distinguished (Figure S2), each with its own computational properties (Naudin et al., 2022c): (i) near-linear, defined by smooth depolarizations or hyperpolarizations from the resting potential (phenotype 1), (ii) bistable, characterized by nonlinear transitions between the resting potential and a depolarized potential, with one resting potential (phenotype 2), and (iii) bistable with two resting potentials (phenotype 3). Naudin et al. (2022c) described a general pattern of the phenotypic evolution of non-spiking neurons as a function of changes in calcium and potassium conductances. As an example, Figure 1 illustrates the phenotypic transitions of non-spiking neurons as calcium conductance (g_{Ca}) decreases through a well-posed retinal cone non-spiking CBM (Kourennyi et al., 2004). To sum up, the wild-type CBM endowed with a phenotype 3 switches to a phenotype 2 and then 1 as g_{Ca} decreases.

The aim of this paper is the development of a numerical procedure to determine a relationship between the dimensionless parameters of the phenomenological non-spiking model (Naudin et al., 2022b) and the calcium conductance of a non-spiking cell, in order to reproduce its phenotypic transitions as g_{Ca} decreases (Figure 1). In other words, the dimensionless parameters of the simple model are expressed as a function of g_{Ca}. In this way, our resulting simple model, called 'conductance-based phenomenological non-spiking model', combines the biological plausibility of CBMs with the high computational efficiency of phenomenological models, and thus may serve as a building block for studying both 'high-level' and 'low-level' functions of non-spiking neural networks. To illustrate our method, the procedure is applied to a model of an intrinsically non-spiking cell type, the retinal cone. Finally, as a proof of concept, we simulate an abstract neural network inspired by the networks of the retina and *C. elegans*, two non-spiking nervous tissues, in which we show that the simple model predicts the same changes in the network output as the CBM for different values of g_{Ca}.

The remainder of the paper is organized as follows. Section 2 describes the evolution of the computational characteristics of the retinal cone CBM as g_{Ca} decreases, that is representative of an ubiquitous and general pattern in non-spiking neurons (Naudin et al., 2022c). Section 3 proposes a numerical procedure to build a phenomenological model

that reproduces the computational characteristic evolution of the retinal cone CBM as g_{Ca} reduces, as described in Section 2. Then, we analyse in Section 4 the dynamics of the resulting model and show that it is well-suited to characterize the phenotypic evolution of the neuron as g_{Ca} decreases. As a proof of concept, we show in Section 5 that the simple model predicts the same effects of conductance variations as the CBM on the ouput of an abstract neural network inspired by both the retina and *C. elegans* networks. Finally, Section 6 discusses the implications on the modeling of the retina and *C. elegans* networks.

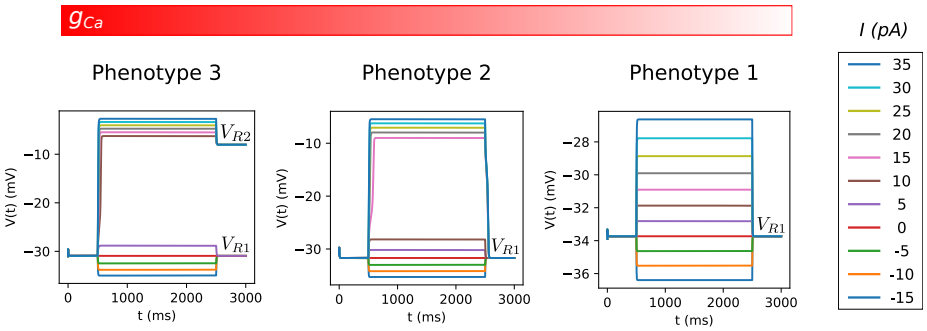

Figure 1: **Phenotypic transitions of the voltage dynamics as g_{Ca} decreases (Naudin et al., 2022c).** A well-posed retinal cone model, with a wild-type phenotype 3, was used as an illustration. A neuron with such a phenotype displays two resting potential values (V_{R1} and V_{R2}). Decreasing g_{Ca} changes the voltage dynamics of the neuron which becomes bistable with only one resting potential (phenotype 2). Finally, the even greater decrease of g_{Ca} leads to the loss of the bistability of the neuron which becomes near-linear (phenotype 1).

2 Preliminaries: evolution of the non-spiking neuron computational characteristics as g_{Ca} decreases

A previous work (Naudin et al., 2022c) determined an ubiquitous and general pattern of non-spiking neuron dynamics as g_{Ca} decreases, illustrated through a well-posed retinal cone CBM (described in Supplementary materials) in Figure 1. It consists in a transition from phenotype 3 to 2 and then to 1 as g_{Ca} decreases. This section aims at describing the computational implications of this phenotypic evolution on the dynamics of the CBM under study.

The evolution of the computational characteristics of a non-spiking CBM can be inferred from the evolution of its steady-state current (SSC). Indeed, the SSC is the underlying data

that confers *all* the qualitative neuro-computational characteristics to non-spiking neurons (Naudin et al., 2022a). Thus, we show in Figure 2.A the evolution of the SSC of the CBM under study as g_{Ca} decreases. The wild-type (WT) SSC (g_{Ca} = 4.92 nS) exhibits a region with negative slope that becomes less and less steep and then disappears as g_{Ca} decreases. This evolution is due to a counterbalanced flow of I_{Ca} and I_K that underlies the negative slope in the SSC of the neuron (Naudin et al., 2022c). This specific voltage-dependence of membrane current is a common mechanism across the animal phyla, including *C. elegans* neurons (Goodman et al., 1998; Mellem et al., 2008; Nicoletti et al., 2019), vertebrate retina cells (Kourennyi et al., 2004; Aoyama et al., 2000; Usui et al., 1996), vertebrate hair cells (Art and Goodman, 1996; Fettiplace, 1987) and thalamocortical neurons (Hughes et al., 1999; Williams et al., 1997). Therefore, the evolution of the SSC under the effect of decreasing g_{Ca} shown in Figure 2.A is representative of a general pattern. This evolution implies a qualitative change in the computational characteristics of non-spiking neurons that we discuss now.

The wild-type SSC (g_{Ca} = 4.92 nS) is N-shaped with two stable zeros (phenotype 3). This provides the neuron with two resting potentials, which gives it a short-term memory capacity: the response of the cell depends on its recent history of activity by storing information about its last input (Figure 2.B). For detailed explanations from a dynamical system viewpoint about the mechanism underlying this phenomenon, we refer to Figure S3 and Naudin et al. (2022c). Then, the negative slope of the SSC becomes less and less steep as g_{Ca} decreases (Figure 2.A), until its local minima becomes positive (*e.g.*, g_{Ca} = 4.22 nS). Therefore, the neuron is still bistable but with only one resting potential (phenotype 2). This implies that the neuron has lost its short-term memory capacity, so the cell's response no longer reflects the history of its inputs and of its activity (Figure 2.C). Finally, an even more decreased value of g_{Ca} (*e.g.*, g_{Ca} = 2.02 nS) gives a monotonic SSC: the neuron becomes near-linear. To sum up, the wild-type neuron with phenotype 3 switches to a phenotype 2, and then from 2 to 1 as g_{Ca} decreases. In other words, the neuron first loses its short-term memory capacity (transition from phenotype 3 to 2), then loses its bistable behavior to a near-linear one (transition from phenotype 2 to 1). One last important evolution of the computational characteristics of the neuron as g_{Ca} reduces is the decrease of the voltage amplitude (Figure 2.D).

The aim of the following section is to propose a procedure that endows a recent and novel non-spiking phenomenological model with the capability to reproduce the evolution of these computational characteristics of the retinal cone CBM as g_{Ca} varies.

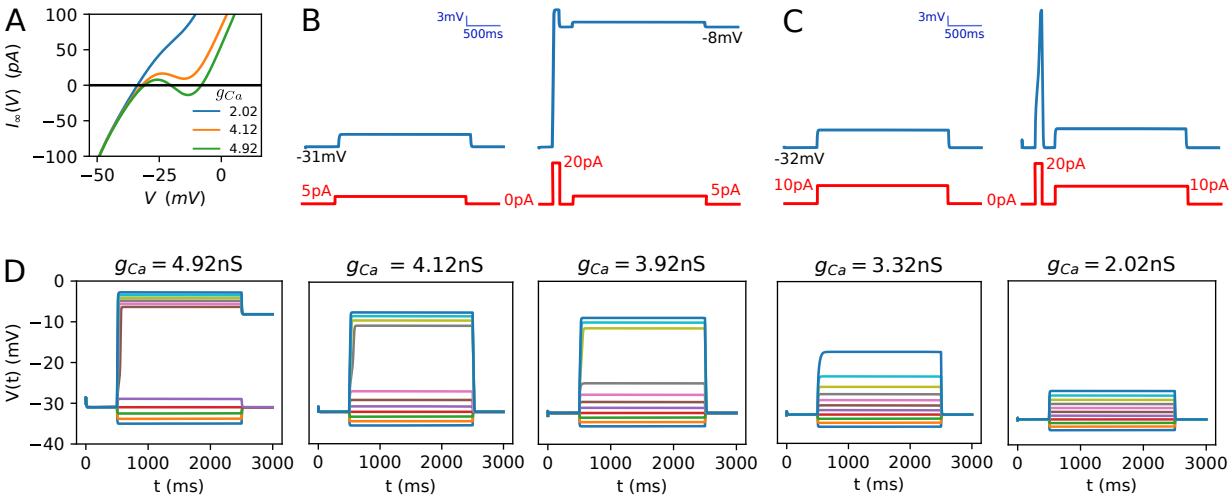

Figure 2: **Evolution of the computational characteristics of the retinal cone CBM as g_{Ca} decreases.** **(A)** SSC curve for three different values of g_{Ca} (4.92 (WT), 4.12, 2.02). **(B)** Short-term memory capacity of the WT phenotype of the CBM (phenotype 3). (Left) A depolarizing current step (5 pA) of 2000 ms duration into the neuron is applied. On cessation of the current step, the voltage stabilizes at its lower resting potential (about −31 mV). (Right) A high transient pulse (20 pA) of 100 ms duration is first injected into the neuron. Its membrane potential then relaxes to its highest resting potential value (approximately −8 mV), and finally stabilizes at about −6 mV in response to the same current injection protocol as before (current injection step at 5 pA under 2000 ms). **(C)** Response of the neuron with a reduced value of g_{Ca} (g_{Ca} = 4.22 nS). Whatever the stimulation protocol used, the neuron stabilizes at a steady-state value of about −29 mV: the response of the neuron no longer reflects the history of its inputs. **(D)** Decrease of the voltage amplitude as g_{Ca} decreases, for a series of current injections starting from −15 pA and increasing to 35 pA by 5 pA increments.

3 Design procedure of the conductance-based phenomenological non-spiking model

This section aims at proposing a methodology to build a simple and lightweight model that reproduces the qualitative evolution of non-spiking neuron dynamics as g_{Ca} decreases, as described in the previous section. The simple model, described in Materials and methods, has the advantage of having a very low computational cost so that one can simulate large-scale neuronal networks in real time (Naudin et al., 2022b), which is more difficult with CBMs due to their complexity (Izhikevich, 2004). Moreover, the simplicity of this model allows a theoretical mathematical analysis to gain insight into neuronal dynamics (Naudin,

2022). Thus, this section proposes a methodology to build such a simple model that reliably predicts the effects of calcium conductance variations on the neuron dynamics. In this way, the model would combine a high computational efficiency and simplicity of mathematical analysis, with the biological plausibility of CBMs.

The methodology is based on the fitting of the evolution of the SSC as g_{Ca} decreases since it determines the neuro-computational features of a non-spiking neuron, as explained above. The fitting of the SSCs by the cubic function

$$f(V) = aV^3 + bV^2 + cV + d \tag{1}$$

of the simple model is based on the Lagrange interpolation theorem. This theorem gives unique combinations of parameters (a, b, c, d) for which the third-degree polynomial f passes through any four given points. Therefore, the aim is to consider four specific points of the SSC to be interpolated by f. Figure 3 shows the two general steps of the procedure, that we apply to the CBM under study in the case of g_{Ca}. The detail of the procedure is given below.

- **Step 1a.** Reproducing the wild-type SSC of the neuron by the cubic function f (1):
  Procedure: To fit the wild-type SSC of the neuron (g_{Ca} = 4.92 nS in our case), we need to consider four points to be interpolated by the cubic function f. Based on the previous section, the four points of the SSC that play a paramount role in the dynamics of the neuron of phenotype 3 are the following:

  - *Resting potentials*: The two stable zeros of the SSC curve, *i.e.* the resting potentials (red points in Figure 4.A).
  - *Local minima and maxima of the SSC:* The local minima and maxima of the SSC curve (blue points in Figure 4.A) because they determine the current injection thresholds at which the voltage jumps to a new plateau.

  Therefore, the parameters (a, b, c, d) of the function f are determined through Lagrange interpolation so that f passes through these four points.
  Output: One vector of parameters (a, b, c, d) for which the cubic function $f(V) = aV^3 + bV^2 + cV + d$ interpolates the four fundamental points of the SCC of the CBM (V_{R1}, V_{R2} and the local minima and maxima of the SSC curve)

- **Step 1b.** Generating four points of the SSC to be interpolated for a series of g_{Ca} associated with phenotypes 3 and 2 by 0.1 nS decrements:
  Procedure: The SSC for phenotypes 3 and 2 is N-shaped (Figure 2.A). Then, the

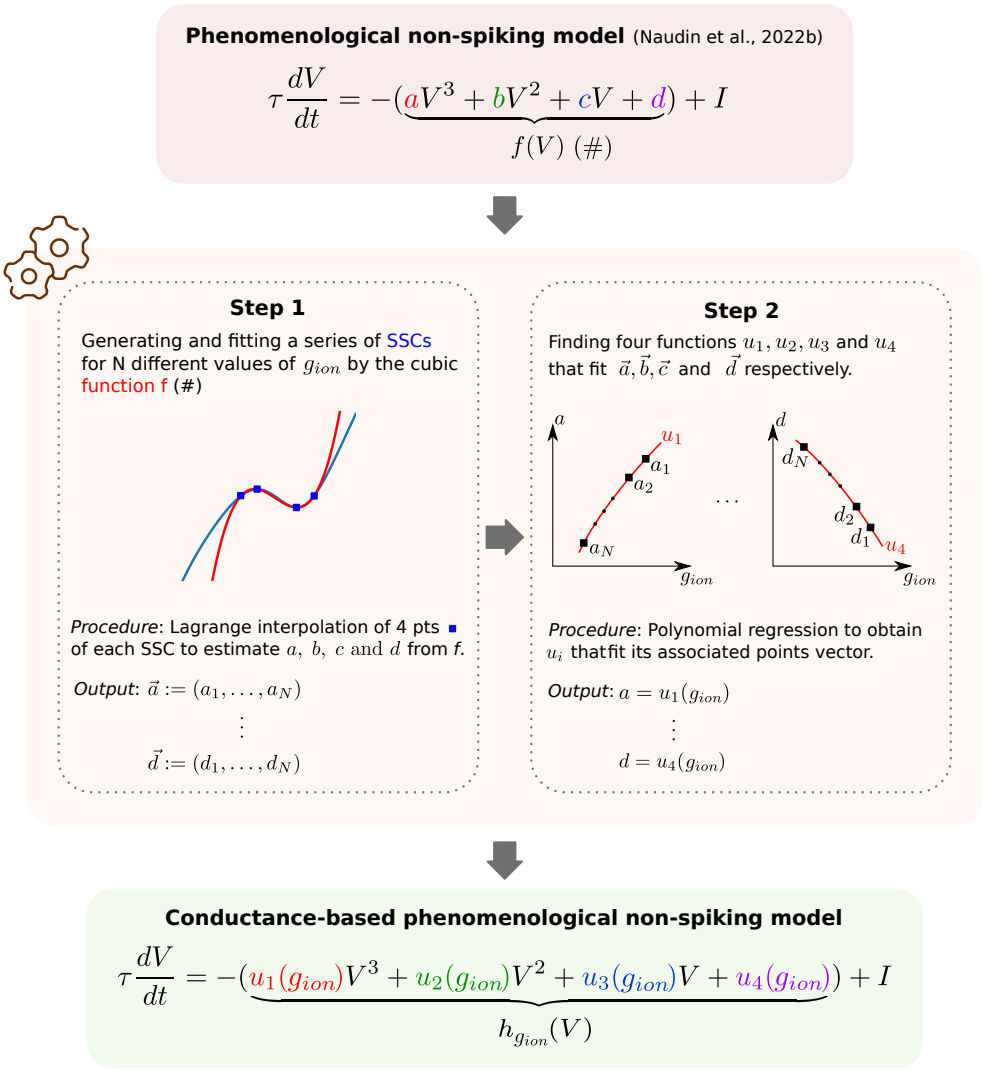

Figure 3: **Overview of the model design procedure. (Top)** The phenomenological non-spiking model (Naudin et al., 2022b) comprises 4 dimensionless parameters a, b, c and d. **(Middle)** The two-stage procedure aims to find a relationship between these parameters and maximal conductances g_{ion} of neurons or CBMs. **(Bottom)** After applying the procedure, the conductance-based phenomenological non-spiking model is obtained and depends only on the g_{ion} parameter.

four points for interpolation by the function f are the local minima and maxima of the SSC curve, and the two points of the lower and upper bounds (−100 pA and 100 pA respectively in this paper):

- *Local minima and maxima of the SSC:* For each SSC of the CBM generated with a new value of g_{Ca} associated with phenotypes 3 and 2, we compute its

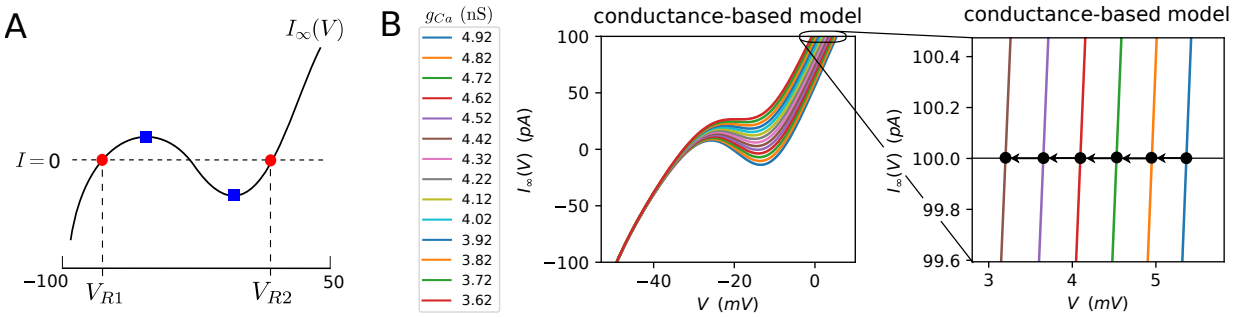

Figure 4: **(A)** The four points of the wild-type SSC to be interpolated by the cubic function of the simple model. Blue squares denote the local minima and maxima of the SSC, representing the current injection thresholds at which the neuron jumps to a new voltage plateau. Red points denote the two stable zeros of the SSC, representing the two resting potentials of the neuron. **(B)** The V-coordinate of the upper bound (100 pA) of the SSC of the CBM decreases more and more as g_{Ca} decreases, which implies a decrease of the voltage amplitude of the neuron as g_{Ca} decreases. The cubic function f of the simple model will then reproduce this pattern in its upper bound.

local minima and maxima, as in Step 1. For the CBM under study, we consider $g_{Ca} \in \{4.82, 4.72, \ldots, 3.62\}$.

- *Upper bound of the SSC:* As can be seen in Figure 4.B, the V-coordinate of the upper bound of the SSC of the CBM decreases more and more as g_{Ca} decreases. This implies the decrease in voltage magnitude as g_{Ca} decreases, a paramount computational feature of the CBM shown in the previous section. To endow the simple model with this characteristic, we generate points in the upper bound that decrease in the V-coordinate in a recusive way from the cubic curve obtained in Step 1.
- *Lower bound of the SSC:* As can be seen in Figure 4, the V-coordinate of the lower bound of the SSC of the CBM remains relatively constant. The cubic function f will seek to preserve such a characteristic.

Output: A series of vector points $\vec{a} := (a_{4.92}, a_{4.82}, \ldots, a_{3.62})$, $\vec{b} := (b_{4.92}, b_{4.82}, \ldots, b_{3.62})$, $\vec{c} := (c_{4.92}, c_{4.82}, \ldots, c_{3.62})$, and $\vec{d} := (d_{4.92}, d_{4.82}, \ldots, d_{3.62})$.

- **Step 2.** Fitting independently the points of $\vec{a}$, $\vec{b}$, $\vec{c}$, and $\vec{d}$ obtained in Step 2:
  Procedure: Finding four functions u_1, u_2, u_3 and u_4 that verify $a = u_1(g_{Ca})$, $b = u_2(g_{Ca})$, $c = u_3(g_{Ca})$ and $d = u_4(g_{Ca})$. In this way, we establish a direct relationship between the parameters a, b, c, and d of the simple model and the calcium

conductance g_{Ca} of the CBM. To that end, the functions u_1, u_2, u_3 and u_4 are considered as polynomials so that polynomial regressions are performed to fit the points of $\vec{a}$, $\vec{b}$, $\vec{c}$ and $\vec{d}$, respectively. We stress the importance to choose polynomials that are not too complex, *i.e.* with degrees that are not too high. Indeed, the SSCs for the phenotype 1 are generated from these functions, *i.e.* for novel values of g_{Ca} not considered during the building of u_1, u_2, u_3 and u_4 through the polynomial regression processes. Therefore, the polynomials should not be too complex to avoid an overfitting of data points which would lead to an inability of the model to generate adequate SSCs for phenotypes 1. In our case, two-degree polynomials u_1, u_2, u_3 and u_4 will be sufficient to obtain good results (see next section).

Input: Vector points $\vec{a} = (a_{4.92}, a_{4.82}, \ldots, a_{3.62})$, $\vec{b} = (b_{4.92}, b_{4.82}, \ldots, b_{3.62})$, $\vec{c} = (c_{4.92}, c_{4.82}, \ldots, c_{3.62})$, and $\vec{d} = (d_{4.92}, d_{4.82}, \ldots, d_{3.62})$.

Output: Four functions u_1, u_2, u_3, and u_4 that verify $a = u_1(g_{Ca})$, $b = u_2(g_{Ca})$, $c = u_3(g_{Ca})$ and $d = u_4(g_{Ca})$, such as we obtain the new model:

$$\tau \frac{dV}{dt} = -h_{g_{Ca}}(V) + I \tag{2}$$

with

$$h_{g_{Ca}}(V) := u_1(g_{Ca})V^3 + u_2(g_{Ca})V^2 + u_3(g_{Ca})V + u_4(g_{Ca}). \tag{3}$$

so that the simple model (2) depends only on the calcium conductance parameter.

In the next section, we show and discuss the results obtained from the procedure proposed in this section applied to the CBM under study.

4 Analysis of the model dynamics

A procedure to build a simple model that reproduces the qualitative evolution of non-spiking neuron dynamics as g_{Ca} evolves has been proposed in the previous section. Since the qualitative evolution of non-spiking neuron dynamics as g_{Ca} evolves is reflected by the evolution of the SSC, the procedure consists in reproducing this evolution of the SSC by the function $h_{g_{Ca}}$ of the model (2). The result of this procedure is shown in Figure 5 in which we compare the evolution of the SSC of the CBM with the function h (Eq. (3)) for different values of g_{Ca}, starting from 4.92 nS and decreasing to 0.02 nS by 0.2 nS decrements. The interpolation functions u_i, $i = 1, \ldots, 4$, of the function h are shown in

Figure S4. In particular, we can observe in Figure 5 that the qualitative evolution of the SSC as g_{Ca} decreases is reproduced with a high fidelity by the cubic function. The purpose of this section is to discuss the implications on the resulting voltage dynamics.

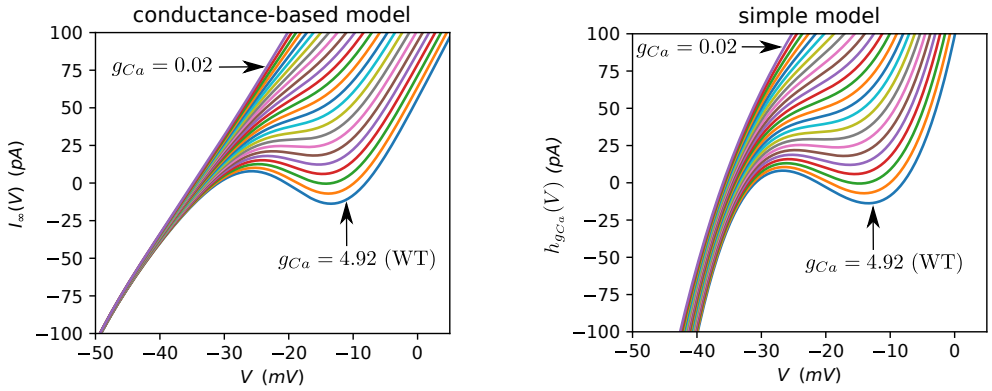

Figure 5: Comparison between the SSC of the CBM and the function h defined in (3) for a series of calcium conductance values g_{Ca} starting from 4.92 nS (WT) and decreasing to 0.02 nS by 0.2 nS decrements.

The first important implication is the occurrence of transitions between different phenotypes for the same g_{Ca} values in the CBM as in the simple model. Indeed, the transition between phenotype 3 and 2 occurs at g_{Ca} = 4.50 nS, both in the CBM and in the simple model. In other words, the CBM and the simple model lose their short-term memory capacity at the same g_{Ca} value. Similarly, the transition between phenotype 2 and 1 occurs at g_{Ca} = 3.59 nS in the CBM, and at g_{Ca} = 3.50 nS in the simple model. Therefore, the loss of bistability in favor of a near-linear type behavior occurs at about the same g_{Ca} values in the CBM as in the simple model.

The second implication stems from the perfect fitting of the function $h_{g_{Ca}}$ with the intermediate values of its associated SSC for any value of g_{Ca} (see Figure 6.A that exemplifies this for g_{Ca} = 4.82 nS). For phenotypes 2 and 3, this implies that the voltage jumps between the down- and up-states of the neuron occur for the same values in the CBM as in the simple model for any value of g_{Ca} (Figure 6.B). That is, the saddle-node bifurcations in the CBM and in the simple model appear for the same values of injection current. Figure S5 shows a representative example (for g_{Ca} = 4.82 nS) of the voltage jump to its up-state in the CBM and in the simple model. In the same way, the CBM and the simple model relax to the same resting values for any value of g_{Ca} (Figure S6).

Furthermore, both in the CBM and in the simple model, we observe a loss of the overall voltage amplitude as g_{Ca} decreases (Figure 6.D), which is a paramount characteristic of the behavior of non-spiking neurons under the effect of calcium conductance decrease. This

observation is partly due to the increase in voltage jump threshold values, as well as the decrease in resting potential values (Figure S6), both resulting from the decrease of g_{Ca}.

Finally, a relative deterioration of the fitting of the SSC for higher and lower values can be observed in Figure 6.A. Nonetheless, it should be noted that substantial noise in the recording of SSCs of non-spiking *C. elegans* neurons can be observed for extreme values, as in the bistable AFD neuron (Figure S7), which is similar to what we obtain (Figure 6.A).

Taken together, the aforementioned observations confirm that the main qualitative features of the raw neuron dynamics are accurately preserved by the simple model. From then on, it can be safely concluded that the simple model is adequate for the description of the neuron behavior as g_{Ca} evolves. In the following section, we consider an abstract neural network inspired by the retina and *C. elegans* non-spiking nervous tissues in which we show, as well, that the simple model predicts the same neuronal changes as the CBM at the network scale.

5 Implementation of a non-spiking neuronal network

In this section, we implement a non-spiking neuronal network inspired by the retina and *C. elegans* networks which are two non-spiking nervous tissues. The neuronal network is composed of three layers (Figure 7.A): (i) a first layer composed of 4 near-linear non-spiking neurons that receive sensory stimuli, (ii) a second layer composed of one bistable non-spiking neuron that could represent mammal bipolar retinal cells (Usui et al., 1996) or the AIA *C. elegans* neuron (Dobosiewicz et al., 2019) for instance, and (iii) a third layer composed of one spiking neuron. This neuron can represent muscles in *C. elegans* which are known to elicit trains of action potentials (Liu et al., 2011), or the retinal ganglion cells – the output neurons of the retina whose axons project to higher processing centers in the brain (Fohlmeister et al., 1990). We use a leaky integrate-and-fire model for the spiking neuron (Gerstner et al., 2014). The near-linear neurons of the first layer are modeled using a near-linear CBM as in Naudin et al. (2022b). Finally, the neuron which composes the second layer is modeled using the CBM or the simple model under study where the parameters have been adjusted according to our procedure (see Section 3).

We consider that all neurons in the first layer receive an identical stimulus input, namely a high transient depolarizing current (20 pA) of 500 ms duration followed by a small depolarizing current step (2 pA) for 1000 ms (Figure 7.A). The resulting electrical signals generated in these sensory neurons are then transmitted to the bistable neuron in the second layer, which itself connects the spiking neuron in the third layer (Figure 7.A).

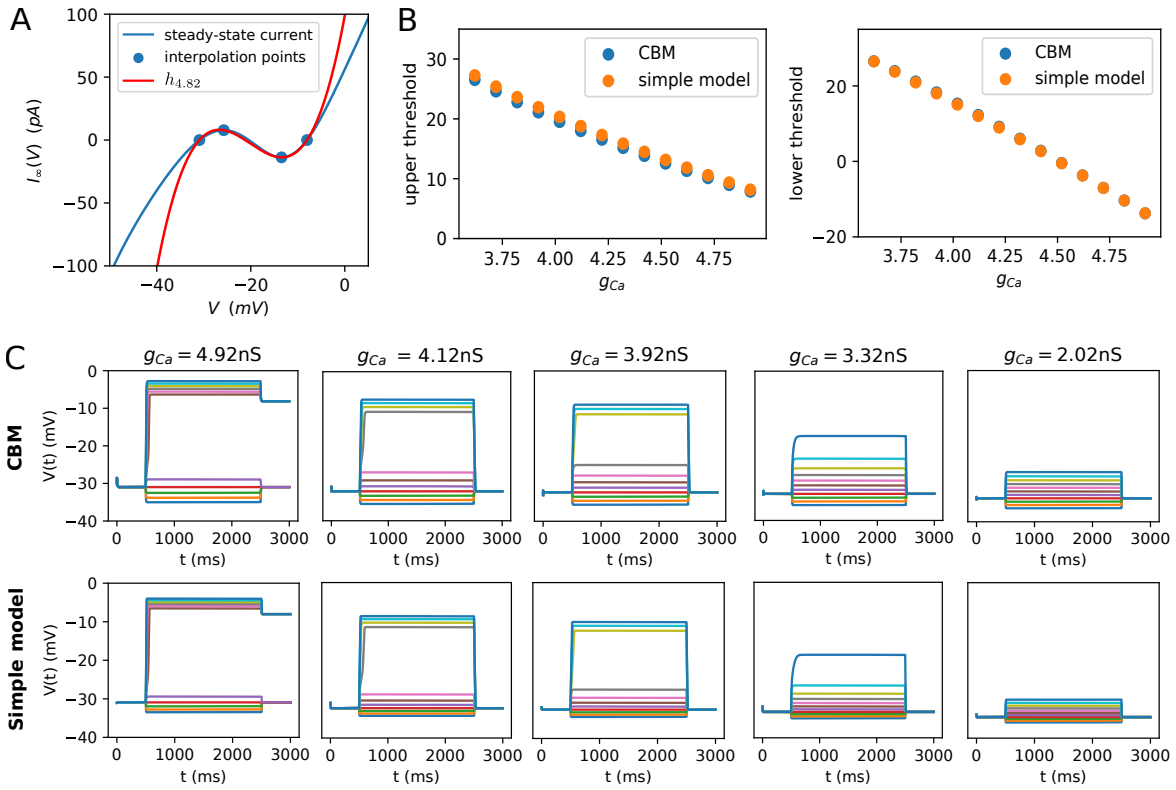

Figure 6: **(A)** Example of SSC (g_{Ca} = 4.82 nS) of the CBM (in blue) against the function $h_{4.82}$ of the simple model (in red) defined in (3). **(B)** Upper and lower threshold of injection currents between the down- and up-states in the CBM and in the simple model. **(C)** Comparison of the voltage amplitude decrease in CBM and in the simple model. For each calcium conductance value, we simulate the models through a series of injection currents starting from −15 pA to 35 pA by 5 pA increments.

The synapses between each layer are considered excitatory and graded, as in *C. elegans* (Lindsay et al., 2011) and in the retina (Dowling, 1987) (see Supplementary materials for the description of the equations). The aim is then to compare the impact of g_{Ca} reduction in the two models on the resulting dynamics of the spiking neuron, the output of the network.

To this end, Figure 7.B compares the dynamics of the spiking neuron output for $g_{Ca} \in \{4.92, 4.22, 2.02\}$ in its presynaptic neuron (i.e. the non-spiking CBM or the conductance-based phenomenological non-spiking model). Whether the network is composed of the CBM or the simple model, the spiking activity of the network output neuron is qualitatively and quantitatively similar for the three different values of g_{Ca}. In particular, the short-term memory capacity of both models for g_{Ca} = 4.92 nS results in a sustained activity of the spiking neuron even after the stimulus ceases (Figure 7.B1). For g_{Ca} = 4.22 nS,

both models have lost their short-term memory capacity (Figure 7.B2), while no activity is observed when g_{Ca} = 2.02 nS (Figure 7.B3). Taken together, these observations suggest that the simple model reliably predicts the conductance changes at the network scale.

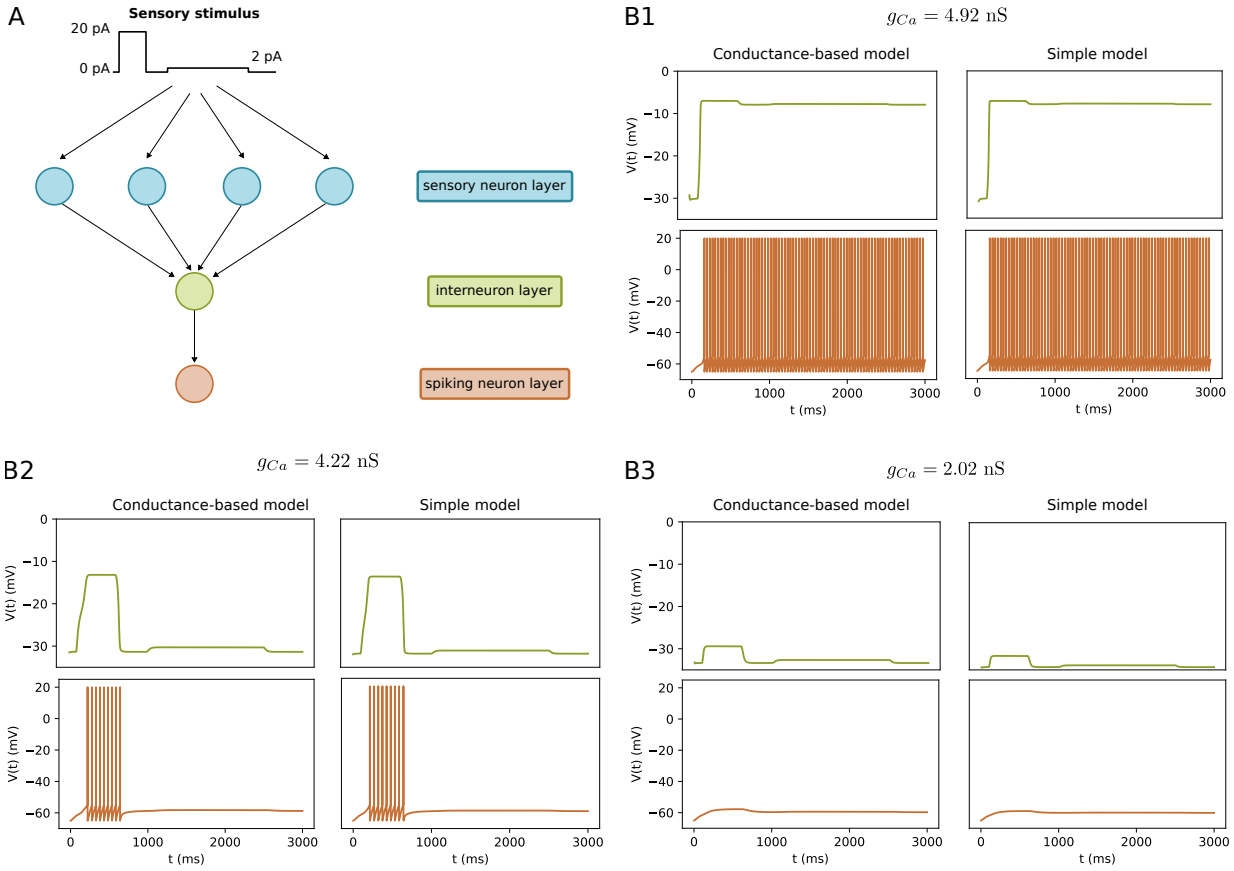

Figure 7: **(A)** Schematic of the neural network made up of three layers: four near-linear sensory neurons, one bistable interneuron, and one spiking output neuron. **(B)** Comparison of the neural network output (spiking activity) when coupled to the simple model or the CBM for three different values of g_{Ca}, each being associated with a distinct phenotype.

6 Discussion

Summary. CBMs and 'phenomenological' models are often used to deal with distinct issues. CBMs are well suited to study 'low-level' functions of nervous systems, depending on physiological microscopic parameters such as ion conductances. Indeed, a CBM is a biophysical representation of a neuron in which every individual parameter and state variable has an established electrophysiological meaning. Nevertheless, the simulation of this type of model is very time-consuming, so the size of neural networks composed of CBMs

that can be studied is inherently limited. In contrast, "phenomenological" models are very lightweight and simple so that one can simulate large-scale networks in real time. But their drawback is the lack of biophysical realism since it describes the macroscopic behavior of neurons regardless the underlying microscopic physiological processes. As a consequence, 'phenomenological' models exhibit dimensionless parameters and are therefore limited to the study of 'higher-level' functions of neural systems. This paper aimed to propose a model for non-spiking neuron dynamics that combines the strengths of the two types of models: the biological plausibility of CBMs with the high computational efficiency of phenomenological models. To do this, a numerical procedure was proposed to establish a relationship between the dimensionless parameters of a non-spiking phenomenological model (Naudin et al., 2022b) and the ion conductances of CBMs or neurons. We applied it to a model of an intrinsically non-spiking cell type, the retinal cone, associated with a decrease in g_{Ca}. We showed that the resulting 'conductance-based phenomenological non-spiking model' was able to accurately depict the phenotypic transitions of non-spiking neurons as g_{Ca} evolves, previously described with CBMs (Naudin et al., 2022c). These cellular properties translated at the network level where the dynamics of our simple model fits the one of the CBM as g_{Ca} varies, resulting in similar network outputs. Therefore, the resulting model combined the biological plausibility of CBMs with the high computational efficiency of phenomenological models, and thus may serve as a building block for studying both 'high-level' and 'low-level' functions of non-spiking neural networks.

Potential applications to the study of the effect of physiological and pathological changes on non-spiking neural network dynamics. Given the importance of ion channels and ion flow for many physiological and pathological functions, both in spiking and in non-spiking neurons, it could be valuable to have a direct relationship with ion conductances when using phenomenological models. This would allow to study various systems and nervous tissues, considering the physiological range of functioning, as well as the pathological variations of their associated ion conductance. Our conductance-based phenomenological non-spiking model was designed in this context, with a particular focus on the calcium conductance variations due to its crucial role in the electrical signal generation in non-spiking neurons.

Indeed, non-spiking neurons, such as *C. elegans* neurons or retinal cells, exhibit a variety of ion channels on their cell membrane, including many voltage-gated calcium and calcium-gated potassium channels (Bargmann, 1998; Taylor et al., 2021; Van Hook et al., 2019). The flow of ions in and out of the cells through these channels provides non-spiking neurons with several crucial physiological properties, including their electrical activity.

In particular, voltage-gated calcium channels are essential in *C. elegans* which lacks the voltage-gated Na^+ channels (Bargmann, 1998) that are usually involved in action potential generation in vertebrates. Likewise, in many retinal cell classes including the cone, rod, bipolar, horizontal and some amacrine cells, voltage-gated Na^+ channels are absent or barely expressed, giving great importance to calcium channels in retinal electrical signal generation (Van Hook et al., 2019). Therefore, it may be particularly relevant to have the ability to assess the impact of calcium gradient variations on neuron behavior as well as on network dynamics.

Furthermore, several mechanisms may alter the "normal" function of ion channels. In particular, many studies show that mutations within genes encoding calcium channels are often associated with various neurological and psychiatric diseases (Andrade et al., 2019). Yet, these ion channels are ubiquitous in the retina cells, whose electrical activity is disturbed as suggested by electrophysiological recordings (electroretinograms) conducted in patients suffering from Parkinson's, Alzheimer's and Huntington's diseases, epilepsy, depression and schizophrenia (Silverstein et al., 2020). In this case, it would also be of particular interest to gain insight into the levels of ion conductance that might lead to pathological behavior.

Taken together, these information confirm that the use of the simple phenomenological model, rather than CBMs, to address these issues is justified both by its minimal computational cost and by its biological plausibility. This original combination allows for the study of precise physiological and pathological changes in a context of large-scale simulations of the retina or *C. elegans* networks.

Acknowledgements

We thank Dr. Mellem and Dr. Liu for their consents to reproduce their experimental data.

We thank the INS2I-CNRS and Loria for their financial support on the ModERN-Psy project.

Code accessibility

The code used in this paper to build the conductance-based phenomenological non-spiking model is available at:
https://gitlab.com/lois76/article-procedure-cbm-phenomenological-model.

Declaration of competing interests

The authors declare no competing interests.

Supplementary materials

Here we present the phenomenological model capable of reproducing the qualitative behaviors of non-spiking neurons, developed in Naudin et al. (2022b). In addition, we recall the role played by the steady-state current (SSC) in the dynamics of non-spiking neurons, since the numerical method developed in this paper fundamentally rely on it.

The phenomenological model

The phenomenological model, developed in Naudin et al. (2022b), is built on the basis of the bifurcation structure of conductance-based models of non-spiking neurons. For the convenience of reading the paper, we present it in this section.

Conductance-based models (CBMs). In CBMs, the dynamics of the membrane potential V is described by a general equation of the form

$$C\frac{\mathrm{d}V}{\mathrm{d}t} = -\sum_{ion} I_{ion} + I \tag{4}$$

where C is the membrane capacitance, $\sum_{ion} I_{ion}$ is the total current flowing accross the cell membrane, and I is an applied current. The currents I_{ion} take the form

$$I_{ion} = g_{ion} m_{ion}^{a} h_{ion}^{b} (V - E_{ion})$$

where m (*resp.* h) denotes the probability for an activation (*resp.* inactivation) gate to be in the open state; a and b are the number of activation and inactivation gates, respectively; g_{ion} is the maximal conductance associated with ion; and E_{ion} is the reversal potential.

Bifurcation dynamics of non-spiking CBMs. In non-spiking CBMs, the SSC curve I_∞ determines the number of equilibra of the system and their values, as well as the bifurcations of the resting state along with the values to which they occur. It takes the general form

$$I_\infty(V) = \sum_{ion} I_{ion\infty}(V) \quad \text{where} \quad I_{ion\infty}(V) = g_{ion} m_{ion\infty}^{a}(V) h_{ion\infty}^{b}(V)(V - E_{ion}) \tag{5}$$

with

$$x_\infty(V) = \frac{1}{1 + \exp\left(\dfrac{V_{1/2}^x - V}{k_x}\right)}, \quad x \in \{m, h\}.$$

where $V_{1/2}^x$ and k_x are constant parameters.

Any stationary point of gating variables $x \in \{m, h\}$ must satisfy $x_* = x_\infty(V_*)$. Replacing this into the first equation on V, fixed points V_* of such models satisfy the equation

$$I_\infty(V_*) = I. \tag{6}$$

In other words, equilibria V_* correspond to the intersection between the SSC I_∞ and a horizontal line $I = c$ where c is a constant. There are two standard steady-state curves I_∞, monotonic and cubic (Figure S1), each involving fundamentally different neurocomputational properties for non-spiking neurons:

- As shown in Figure S1.A, CBMs with a monotonic SSC only have one equilibrium for any value of I. Non-spiking neurons with such a SSC display a near-linear behavior characterized by smooth depolarizations or hyperpolarizations from the resting potential, such as the RIM neuron (Figure S2).

- As shown in Figure S1.B, a N-shaped curve leads to a saddle-node bifurcation. When $I = c_1$, there are 3 equilibria, noted $V_{1*}^{c_1}$, $V_{2*}^{c_1}$ and $V_{3*}^{c_1}$. Increasing I results in coalescence of two equilibria (the stable $V_{1*}^{c_1}$ with the unstable $V_{2*}^{c_1}$). The value $I = c_2$, at which the equilibria coalesce, is called the *bifurcation value*. For this value of I, there exist 2 equilibria. For $I > c_2$, the system has only one equilibrium (*e.g.* $I = c_3$). In summary, when the parameter I increases, a stable and an unstable equilibrium approach, coalesce, and then annihilate each other. Non-spiking neurons with a N-shaped SSC display a bistable behavior characterized by a voltage jump between the resting potential and a depolarized potential of higher voltage, such as the AFD neuron (Figure S2).

Therefore, it can be stated that the SSC determines the bifurcation structure of non-spiking neurons and the equilibrium values of their graded responses to particular stimuli.

The simple model. Let V represent the membrane potential of a neuron. The simple model takes the general form

$$\tau \frac{\mathrm{d}V}{\mathrm{d}t} = -f(V) + I \tag{7}$$

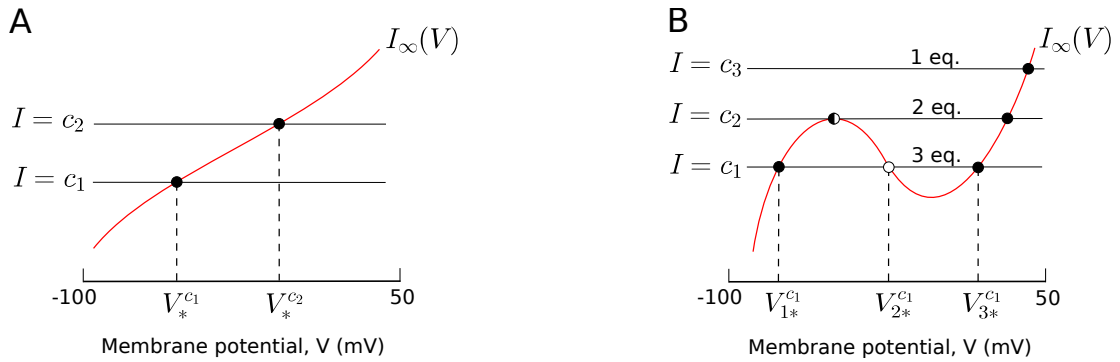

Figure S1: Two typical shapes of the SSC $V \to I_\infty(V)$, in red. Intersections of I_∞ and horizontal line $I = c$ (with c constant) correspond to equilibria of the system. We denote stable equilibria as filled circles ●, unstable equilibria as open circles ○ and saddle-node equilibria as ◐. **(A)** Monotonic SSC. $V_*^{c_1}$ and $V_*^{c_2}$ correspond to equilibria for a current injection $I = c_1$ and $I = c_2$ respectively. **(B)** N-shaped SSC. The number of equilibria of the system depends on the value of I. For the sake of readibility, we highlight equilibria only for $I = c_1$, noted $V_{1*}^{c_1}$, $V_{2*}^{c_1}$ and $V_{3*}^{c_1}$.

with f a cubic function which reads as

$$f(V) = aV^3 + bV^2 + cV + d. \tag{8}$$

The function f plays the same role in the dynamics of the model (7) as the SSC I_∞ in CBMs (4). Indeed, fixed points V_* of model (7) satisfy

$$f(V_*) = I$$

so that the shape of f determines the neuro-computational features of the non-spiking model: a monotonic shape involves a near-linear behavior of the model, while a N-shape implies a bistable one with the occurrence of two saddle-node bifurcations. Therefore, the model proposes a simple cubic expression (8) thats plays the same role as the complex SSC expression (5) of CBMs. Parameters a, b, c and d are dimensionless and are estimated in order to fit the experimental SSC. Parameter τ describes the *constant* time for which V reaches its equilibrium value V_*. This parameter can be either hand-tuned or estimated from experimental voltage.

Conductance-based model of the retinal cone

The conductance-based model of the canonical bistable cell is based on the retinal cone cell built in Kourennyi et al. (2004). It has four ion currents: a calcium current (I_{Ca}), a hyperpolarization-activated current (I_h), a delayed rectifying potassium current (I_{Kv}), and a leak current (I_L). The parameters are expressed in the following units: mV (voltage), pA (current), nS (conductance), and ms (time). The membrane capacitance (C) is set to 16 nF. We denote by g_{ion} the maximal conductance (namely the conductance of the channel when all the gates are open), and E_{ion} the reversal potential, that is, the potential at which the ion current reverses its direction. Leak current is classically described as $I_L = g_L(V - E_L)$ and the remaining currents are described in Table S1.

Ion current (I_{ion})	$\alpha_{ion}(V)$ and $\beta_{ion}(V)$ rates	g_{ion} and E_{ion}
$I_{Ca} = g_{Ca} m_{Ca} h_{Ca} (V - E_{Ca})$	$\alpha_{Ca}(V) = 3.1\, e^{(V+16.6)/11.4}$	$g_{Ca} = 4.92$
$\frac{dm_{Ca}}{dt} = \alpha_{Ca}(1 - m_{Ca}) - \beta_{Ca} m_{Ca}$	$\beta_{Ca}(V) = 3.1\, e^{(-V-16.6)/11.4}$	$E_{Ca} = 40$
$I_h = g_h(1 - (1 + 3m_h)(1 - m_h)^3)(V - E_h)$	$\alpha_{m_h}(V) = \frac{18}{(1 + e^{(V+88)/12})}$	$g_h = 3.5$
$\frac{dm_h}{dt} = \alpha_{m_h}(1 - m_h) - \beta_{m_h} m_h$	$\beta_{m_h}(V) = \frac{18}{(1 + e^{-(V+18)/19})}$	$E_h = -32.5$
$I_{Kv} = g_{Kv} m_{Kv}^3 h_{Kv} (V - E_K)$	$\alpha_{m_{Kv}}(V) = \frac{5(V - 100)}{(1 - e^{-(V-100)/42})}$	$g_{Kv} = 2$
$\frac{dm_{Kv}}{dt} = \alpha_{m_{Kv}}(1 - m_{Kv}) - \beta_{m_{Kv}} m_{Kv}$	$\beta_{m_{Kv}}(V) = 9\, e^{(20-V)/40}$	$E_{Kv} = -80$
$\frac{dh_{Kv}}{dt} = \alpha_{h_{Kv}}(1 - h_{Kv}) - \beta_{h_{Kv}} h_{Kv}$	$\alpha_{h_{Kv}}(V) = 0.15\, e^{-V/22}$	
	$\beta_{h_{Kv}}(V) = \frac{0.4125}{(1 + e^{(10-V)/7})}$	

Table S1: Summary of ion currents composing the generic bistable model.

Network models

The graded synaptic model used in this paper is described in Wicks et al. (1996), which is given by

$$I_{syn} = g_{syn} s (V_i - E_{syn})$$

where g_{syn} is the maximal synaptic conductance, and E_{syn} is the reversal potential for the synaptic current, set to 0 mV for excitatory synapses. The dynamics of the variable s is

given by

$$\frac{ds}{dt} = \frac{s_\infty(V_j) - s}{\tau_s}$$

where

$$s_\infty(V_j) = \frac{1}{1 + \exp\left(\frac{V_{1/2}^s - V_j}{V_{slope}}\right)}$$

We set the parameter values as follows: $g_{syn} = 0.2$ nS, $V_{1/2}^s = -10$ mV, $V_{slope} = 10$ mV, and $\tau_s = 10$ ms.

Supplementary figures

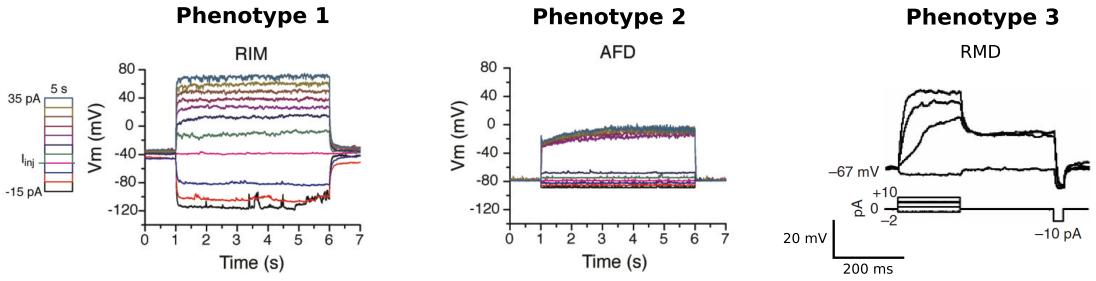

Figure S2: Experimental voltage examples from *C. elegans* of each phenotype for a series of current injections starting from −15pA and increasing to 35pA by 5pA increments for the RIM and AFD neurons, and starting from −2pA and increasing to 10pA by 3pA increments for the RMD neuron. Phenotype 1 refers to near-linear neurons, phenotype 2 to bistable neurons with one resting potential, and phenotype 3 to bistable neurons with two resting potentials. The experimental data of the RIM and AFD neurons have been reproduced from Naudin et al. (2022a), and from Mellem et al. (2008) for the RMD neuron with the consent of the authors.

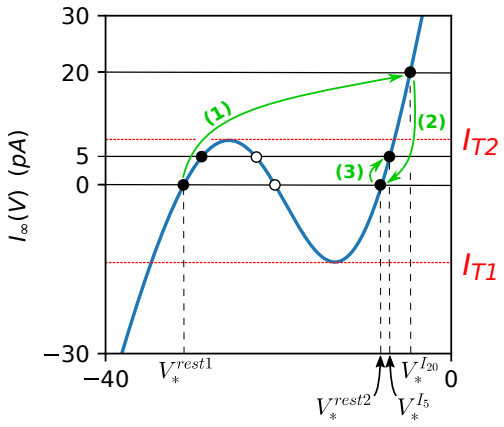

Figure S3: Diagram explaining the short-term memory capacity of a neuron with a phenotype 3. I_{T1} (resp. I_{T2}) denotes the injection current thresholds at which the neuron jumps to its upper (resp. lower) voltage plateau. (1) A brief transient stimulus ($20 > I_{T2}$ pA) is applied and the voltage converges to $V_*^{I_{20}}$. (2) The stimulus ceases so that the voltage relaxes to V_*^{rest2} which is the new voltage initial condition. (3) A new depolarizing current step (5pA) is applied and the voltage goes to $V_{2*}^{I_5}$ and not $V_{1*}^{I_5}$ since V_*^{rest2} now belongs to the basin of attraction of $V_{2*}^{I_5}$. This figure has been reproduced from Naudin et al. (2022c) with the consent of the authors.

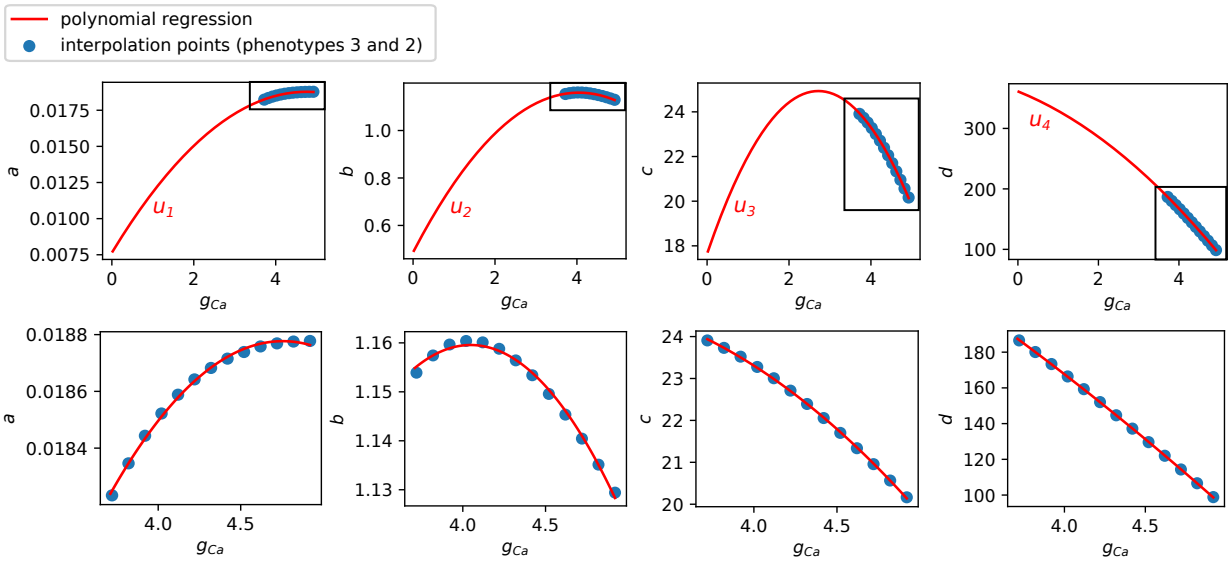

Figure S4: **(Top)** Two-degree polynomials u_i, $i = 1, \ldots, 4$, built from the polynomial regression of blue points. These points are generated following Step 1 and Step 2 of the procedure described in Section 3. **(Bottom)** Zoom of the rectangles in (Top).

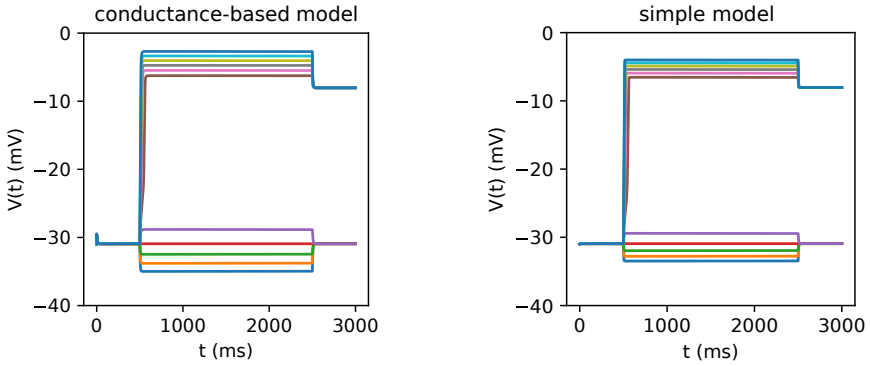

Figure S5: Comparison of voltage dynamics between CBM and the conductance-based phenomenological non-spiking model for g_{Ca} = 4.82nS for a series of injection currents starting from −15pA and increasing to 35pA by 5pA increments.

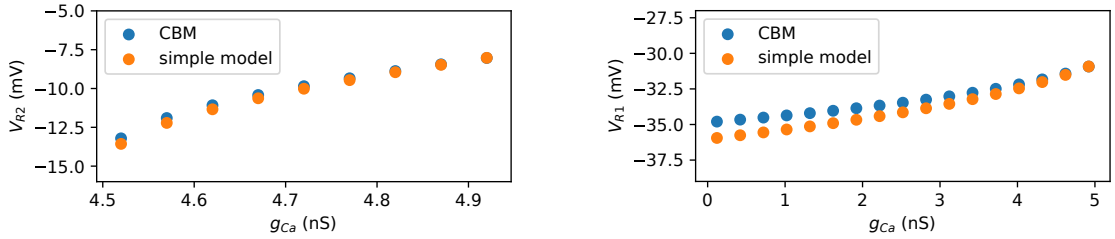

Figure S6: Comparison of the resting potential values (V_{R1} and V_{R2}) for various values of g_{Ca} in the CBM and in the simple model.

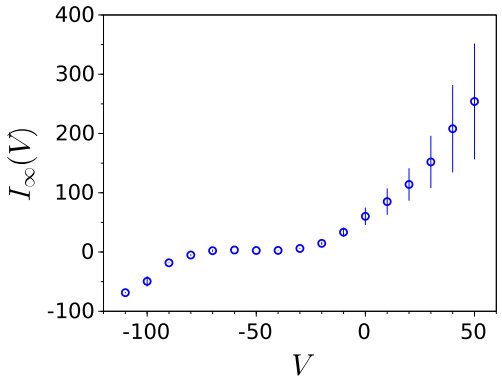

Figure S7: SSC of the AFD neuron obtained from averaged voltage-clamp recordings (n = 3) (Liu et al., 2018).

References

A. Andrade, A. Brennecke, S. Mallat, J. Brown, J. Gomez-Rivadeneira, N. Czepiel, and L. Londrigan. Genetic associations between voltage-gated calcium channels and psychiatric disorders. *International journal of molecular sciences*, 20(14):3537, 2019.

T. Aoyama, Y. Kamiyama, S. Usui, R. Blanco, C. F. Vaquero, and P. de la Villa. Ionic current model of rabbit retinal horizontal cell. *Neuroscience Research*, 37(2):141–151, 2000.

J. Art and M. Goodman. Ionic conductances and hair cell tuning in the turtle cochlea a. *Annals of the New York Academy of Sciences*, 781(1):103–122, 1996.

C. I. Bargmann. Neurobiology of the caenorhabditis elegans genome. *Science*, 282(5396): 2028–2033, 1998.

S. S. Bidaye, T. Bockemühl, and A. Büschges. Six-legged walking in insects: how cpgs, peripheral feedback, and descending signals generate coordinated and adaptive motor rhythms. *Journal of neurophysiology*, 119(2):459–475, 2018.

R. Brette. What is the most realistic single-compartment model of spike initiation? *PLoS computational biology*, 11(4):e1004114, 2015.

M. Burrows, G. Laurent, and L. Field. Proprioceptive inputs to nonspiking local interneurons contribute to local reflexes of a locust hindleg. *Journal of Neuroscience*, 8(8): 3085–3093, 1988.

R. Davis and A. Stretton. Passive membrane properties of motorneurons and their role in long-distance signaling in the nematode ascaris. *Journal of Neuroscience*, 9(2):403–414, 1989a.

R. E. Davis and A. Stretton. Signaling properties of ascaris motorneurons: graded active responses, graded synaptic transmission, and tonic transmitter release. *Journal of Neuroscience*, 9(2):415–425, 1989b.

M. Dobosiewicz, Q. Liu, and C. I. Bargmann. Reliability of an interneuron response depends on an integrated sensory state. *Elife*, 8:e50566, 2019.

J. E. Dowling. *The retina: an approachable part of the brain*. Harvard University Press, 1987.

C. Eliasmith and O. Trujillo. The use and abuse of large-scale brain models. *Current opinion in neurobiology*, 25:1–6, 2014.

G. B. Ermentrout and D. H. Terman. *Mathematical foundations of neuroscience*, volume 35. Springer Science & Business Media, 2010.

R. Fettiplace. Electrical tuning of hair cells in the inner ear. *Trends in Neurosciences*, 10 (10):421–425, 1987.

G. D. Field and E. Chichilnisky. Information processing in the primate retina: circuitry and coding. *Annu. Rev. Neurosci.*, 30:1–30, 2007.

R. FitzHugh. Impulses and physiological states in theoretical models of nerve membrane. *Biophysical journal*, 1(6):445–466, 1961.

J. Fohlmeister, P. Coleman, and R. F. Miller. Modeling the repetitive firing of retinal ganglion cells. *Brain research*, 510(2):343–345, 1990.

W. Gerstner, W. M. Kistler, R. Naud, and L. Paninski. *Neuronal dynamics: From single neurons to networks and models of cognition*. Cambridge University Press, 2014.

F. Giovannini, B. Knauer, M. Yoshida, and L. Buhry. The can-in network: A biologically inspired model for self-sustained theta oscillations and memory maintenance in the hippocampus. *Hippocampus*, 27(4):450–463, 2017.

M. B. Goodman, D. H. Hall, L. Avery, and S. R. Lockery. Active currents regulate sensitivity and dynamic range in c. elegans neurons. *Neuron*, 20(4):763–772, 1998.

T. Górski, D. Depannemaecker, and A. Destexhe. Conductance-based adaptive exponential integrate-and-fire model. *Neural Computation*, 33(1):41–66, 2021.

A. L. Hodgkin and A. F. Huxley. A quantitative description of membrane current and its application to conduction and excitation in nerve. *The Journal of physiology*, 117(4): 500–544, 1952.

S. W. Hughes, D. W. Cope, T. I. Tóth, S. R. Williams, and V. Crunelli. All thalamocortical neurones possess a t-type ca2+ 'window' current that enables the expression of bistability-mediated activities. *The Journal of physiology*, 517(3):805–815, 1999.

E. M. Izhikevich. Simple model of spiking neurons. *IEEE Transactions on neural networks*, 14(6):1569–1572, 2003.

E. M. Izhikevich. Which model to use for cortical spiking neurons? *IEEE transactions on neural networks*, 15(5):1063–1070, 2004.

D. E. Kourennyi, X.-d. Liu, J. Hart, F. Mahmud, W. H. Baldridge, and S. Barnes. Reciprocal modulation of calcium dynamics at rod and cone photoreceptor synapses by nitric oxide. *Journal of neurophysiology*, 92(1):477–483, 2004.

P. E. Latham, B. Richmond, P. Nelson, and S. Nirenberg. Intrinsic dynamics in neuronal networks. i. theory. *Journal of neurophysiology*, 83(2):808–827, 2000.

G. Laurent and M. Burrows. Intersegmental interneurons can control the gain of reflexes in adjacent segments of the locust by their action on nonspiking local interneurons. *Journal of Neuroscience*, 9(9):3030–3039, 1989.

L. Lemaire, M. Desroches, M. Krupa, L. Pizzamiglio, P. Scalmani, and M. Mantegazza. Modeling nav1. 1/scn1a sodium channel mutations in a microcircuit with realistic ion concentration dynamics suggests differential gabaergic mechanisms leading to hyperexcitability in epilepsy and hemiplegic migraine. *PLoS Computational Biology*, 17(7): e1009239, 2021.

T. H. Lindsay, T. R. Thiele, and S. R. Lockery. Optogenetic analysis of synaptic transmission in the central nervous system of the nematode caenorhabditis elegans. *Nature communications*, 2(1):1–9, 2011.

P. Liu, Q. Ge, B. Chen, L. Salkoff, M. I. Kotlikoff, and Z.-W. Wang. Genetic dissection of ion currents underlying all-or-none action potentials in c. elegans body-wall muscle cells. *The Journal of physiology*, 589(1):101–117, 2011.

Q. Liu, P. B. Kidd, M. Dobosiewicz, and C. I. Bargmann. C. elegans awa olfactory neurons fire calcium-mediated all-or-none action potentials. *Cell*, 175(1):57–70, 2018.

S. R. Lockery, M. B. Goodman, and S. Faumont. First report of action potentials in a c. elegans neuron is premature. *Nature neuroscience*, 12(4):365–366, 2009.

J. E. Mellem, P. J. Brockie, D. M. Madsen, and A. V. Maricq. Action potentials contribute to neuronal signaling in c. elegans. *Nature neuroscience*, 11(8):865–867, 2008.

L. Naudin. Biological emergent properties in non-spiking neural networks. *AIMS Mathematics*, 7(10):19415–19439, 2022.

L. Naudin, J. L. Jiménez Laredo, Q. Liu, and N. Corson. Systematic generation of biophysically detailed models with generalization capability for non-spiking neurons. *PloS one*, 17(5):e0268380, 2022a.

L. Naudin, J. L. J. Laredo, and N. Corson. A simple model of nonspiking neurons. *Neural Computation*, 34(10):2075–2101, 2022b.

L. Naudin, L. Raison-Aubry, and L. Buhry. A general pattern of non-spiking neuron dynamics under the effect of potassium and calcium channel modifications. *Journal of Computational Neuroscience*, pages 1–14, 2022c.

M. Nicoletti, A. Loppini, L. Chiodo, V. Folli, G. Ruocco, and S. Filippi. Biophysical modeling of c. elegans neurons: Single ion currents and whole-cell dynamics of awcon and rmd. *PloS one*, 14(7):e0218738, 2019.

T. O'Leary, A. C. Sutton, and E. Marder. Computational models in the age of large datasets. *Current opinion in neurobiology*, 32:87–94, 2015.

P. Poirazi and A. Papoutsi. Illuminating dendritic function with computational models. *Nature Reviews Neuroscience*, pages 1–19, 2020.

A. Roberts and B. M. Bush. *Neurones without impulses: their significance for vertebrate and invertebrate nervous systems*, volume 6. Cambridge University Press, 1981.

S. M. Silverstein, D. L. Demmin, J. B. Schallek, and S. I. Fradkin. Measures of retinal structure and function as biomarkers in neurology and psychiatry. *Biomarkers in Neuropsychiatry*, 2:100018, 2020.

G. D. Smith, C. L. Cox, S. M. Sherman, and J. Rinzel. Fourier analysis of sinusoidally driven thalamocortical relay neurons and a minimal integrate-and-fire-or-burst model. *Journal of neurophysiology*, 83(1):588–610, 2000.

S. R. Taylor, G. Santpere, A. Weinreb, A. Barrett, M. B. Reilly, C. Xu, E. Varol, P. Oikonomou, L. Glenwinkel, R. McWhirter, et al. Molecular topography of an entire nervous system. *Cell*, 184(16):4329–4347, 2021.

S. Usui, A. Ishihaiza, Y. Kamiyama, and H. Ishii. Ionic current model of bipolar cells in the lower vertebrate retina. *Vision research*, 36(24):4069–4076, 1996.

M. J. Van Hook, S. Nawy, and W. B. Thoreson. Voltage-and calcium-gated ion channels of neurons in the vertebrate retina. *Progress in retinal and eye research*, 72:100760, 2019.

S. R. Wicks, C. J. Roehrig, and C. H. Rankin. A dynamic network simulation of the nematode tap withdrawal circuit: predictions concerning synaptic function using behavioral criteria. *Journal of Neuroscience*, 16(12):4017–4031, 1996.

S. R. Williams, T. I. Toth, J. P. Turner, S. W. Hughes, and V. Crunelli. The 'window'component of the low threshold ca2+ current produces input signal amplification and bistability in cat and rat thalamocortical neurones. *The Journal of physiology*, 505 (3):689–705, 1997.